Nanoscale

PAPER

View Article Online
View Journal | View Issue

Cite this: *Nanoscale*, 2014, **6**, 14380

Probing the size of proteins with glass nanopores†

L. J. Steinbock,‡[a] S. Krishnan,‡[b] R. D. Bulushev,[a] S. Borgeaud,[c] M. Blokesch,[c] L. Feletti[a] and A. Radenovic*[a]

Received 28th August 2014,
Accepted 1st October 2014

DOI: 10.1039/c4nr05001k

www.rsc.org/nanoscale

Single molecule studies using nanopores have gained attention due to the ability to sense single molecules in aqueous solution without the need to label them. In this study, short DNA molecules and proteins were detected with glass nanopores, whose sensitivity was enhanced by electron reshaping which decreased the nanopore diameter and created geometries with a reduced sensing length. Further, proteins having molecular weights (MW) ranging from 12 kDa to 480 kDa were detected, which showed that their corresponding current peak amplitude changes according to their MW. In the case of the 12 kDa ComEA protein, its DNA-binding properties to an 800 bp long DNA molecule was investigated. Moreover, the influence of the pH on the charge of the protein was demonstrated by showing a change in the translocation direction. This work emphasizes the wide spectrum of detectable molecules using nanopores from glass nanocapillaries, which stand out because of their inexpensive, lithography-free, and rapid manufacturing process.

Introduction

Single molecule DNA detection using the resistive pulse technique and solid-state nanopores was accomplished in 2001 by Li *et al.*, partly because of its stability and the long length of commercially available DNA.[1,2] Proteins, which are normally shorter and more fragile than DNA, were detected several years later.[3] Since then, numerous studies were published on the factors influencing the folding of proteins when they translocated,[4,5] including pH,[6–8] applied potential,[9] nanopore diameter,[10,11] potassium chloride (KCl) concentration,[12] temperature,[13] and denaturing agents such as urea.[7,14] Some studies investigated the influence of lipids and the antibody coating of nanopores which makes the nanopore specific for the passing molecule and delays their translocation time.[15–18] Biologically motivated protein detection mechanisms were tested by attaching DNA and RNA aptamers to nanopores in order to selectively detect proteins.[19–22] The quantity and spectrum of research demonstrates that protein detection with nanopores is a viable technique currently attracting academic interest. Because of its sensitivity and parallelization ability, even the sequencing of long DNA strands are now possible.[23]

The limits with other techniques such as size-exclusion chromatography (SEC) are its susceptibility to clogging and its reliance on salt solutions and charged analytes. Although SEC is not a single molecule technique, its reliability and good sensitivity for the shape and charge of a molecule represents the gold standard for protein detection using glass nanopores.

A new subclass within solid-state nanopores are glass nanocapillaries made from laser pulled glass capillaries which can also detect single DNA molecules.[24,25] Their fabrication is fast, cost-effective, and does not require a clean room.[26–28] Moreover, they can be easily combined with optical tweezers and segmented flow microfluidics which opens novel avenues to measure forces and develop new lab-on-the-chip applications.[29–34]

In the beginning, classical solid-state nanopores and glass nanocapillaries were used to detect DNA.[24] Yet, protein sensing is equally interesting because the market of proteomics which includes techniques like mass spectrometry and 2D gel electrophoresis for weight determination, is growing. It will represent several billion dollars in 2014.[35] Therefore, the presentation of an alternative detection method for a protein's molecular weight with glass nanopores would be a step forward for commercial applications of the resistive pulse technique (Fig. 1a). In 2013, Li *et al.* succeeded for the first time in detecting proteins using laser-pulled glass nanocapillaries for molecular weights ranging from 14 to 465 kDa.[36] These experiments were performed at one single pH, and with different nanocapillaries for each protein. Due to low signal-to-noise ratios (SNR), the detection of the majority of the proteins was made possible by increasing the Bessel filter frequency from 10 to 50 kHz.

The Merlin (Zeiss) Scanning Electron Microscope (SEM) allowed imaging of every glass nanopore before the experiment

[a]*Laboratory of Nanoscale Biology, Institute of Bioengineering, School of Engineering, EPFL, 1015 Lausanne, Switzerland. E-mail: aleksandra.radenovic@epfl.ch*
[b]*Technical University of Dresden, 01069, Germany*
[c]*Laboratory of Molecular Microbiology, Global Health Institute, School of Life Sciences, EPFL, 1015 Lausanne, Switzerland*

†Electronic supplementary information (ESI) available. See DOI: 10.1039/c4nr05001k

‡Both authors contributed equally.

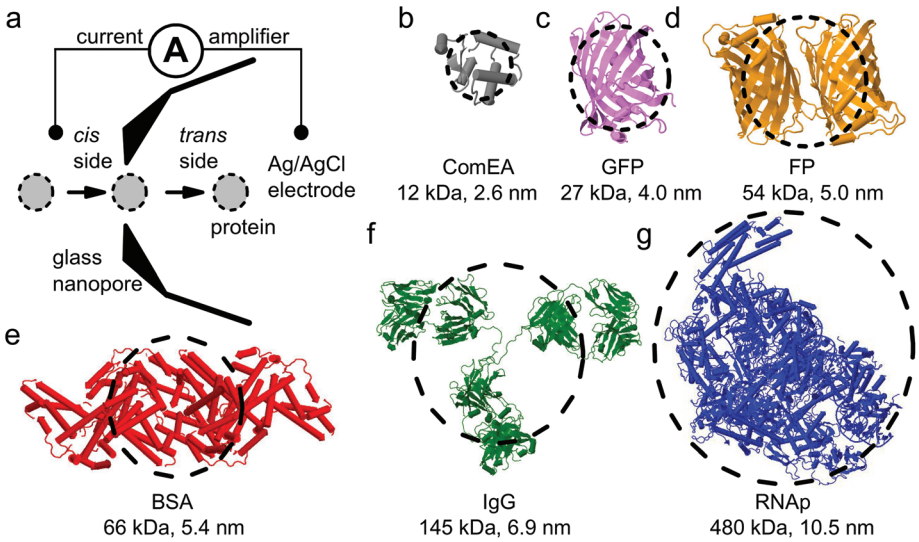

Fig. 1 (a) Schematic of the setup showing a glass nanopore positioned between two Ag/AgCl electrodes. The left electrode is in the *cis* chamber and it is grounded. The second working electrode is behind the conical part of the glass nanopore and is connected to the current amplifier, which allows the application of potentials ranging from −1 to +1 V. (b) Three dimensional structure of a competence protein ComEA-related protein (PDB ID 2DUY). Visualizing the used ComEA protein. The dashed circle represents the size of the protein simplified as a sphere, whose diameter is displayed besides the molecular weight. (c) GFP (PDB ID 1EMA) showing the distinctive barrel structure. Note that the proteins are not in correct scaling but the dashed circles are. (d) The fusion protein (FP) constituted of the dimer PSCFP2-PAMCherry1 is represented by the PDB ID 2OKY, which has a similar structure. Its expression and purification is described in the ESI.† (e) Structure of BSA (PDB ID 4F5S). (f) IgG antibody against anti-his tag mimicked by the PDB ID 1IGT. (g) RNA polymerase (RNAp) protein used in a previous publication (PDB ID 3IYD).[40]

without the requirement of a coating with a conducting layer. This only permitted the use of glass nanopores with slightly bigger diameters than the target protein, thus improving the signal to noise ratio (Fig. 1a).[37] Moreover, SEM allowed the glass nanopore of the nanocapillary to be shrunken to any size within minutes, permitting a rapid fabrication.[38] In contrast to the experiment conducted by Li *et al.*, the improved SNR did not require an increase in the Bessel filter frequency to 50 kHz, but allowed the detection of the protein at a constant Bessel filter frequency of 10 kHz. A varying Bessel filter frequency changes the amplitude and duration of the current decrease which is caused by the translocating particle.[36,39] Different Bessel filters complicate the comparison of the results of different-sized proteins. Since the goal was to detect a wide range of proteins and examine if their respective current decrease agreed with their molecular weight when translocated through the glass nanopore, a constant Bessel filter frequency was essential. Moreover, we show that the inversion of the translocation direction is caused by a change in the pH values. Lastly, our results show the detection of several proteins and DNA with one single glass nanopore.

In this study a size range of proteins starting from 12 to 480 kDa (Fig. 1b–g) was used. All proteins had a negative charge at pH 8 estimated by the ProteinCalculator v3.4 software (see ESI Table 1†). The fractional conductance blockade (G^*) was calculated by dividing the concatenated current traces by the applied potential (U) and the conductance of the cell (G). The G^* histogram was fitted by a Gauss function to determine the position of the protein peak. G^* equals the fractional current amplitude for the nanopore for perfectly linear IV-curves and is used for the investigation of spherical particles using the resistive pulse technique.[41] In contrast to the equivalent charge deficit (e.c.d.), the fractional current amplitude used by Wanunu's and other groups was more appropriate when working with spherical particles like proteins. The e.c.d. is better suited for long polymers like DNA with a length which is a multiple of the persistence length (>1000 bp). In addition, the lower sample and Bessel frequency of the Axon current amplifier compared to devices such as the Chimera (Chimera Instruments, NY, USA) decreases the event duration and would result in an underestimation of the e.c.d. value of small proteins.[36,39]

The effect of different pH values on the translocation potential of proteins was further investigated. Their surface charge becomes either negative or positive depending on the pH and the isoelectric point (pI) values. In the case of BSA (pI 4.7) at pH 2.5 and 8 the protein translocated at the opposite potentials of −0.8 V and +0.8 V, respectively.[3]

Another experiment explored the DNA-binding capabilities of ComEA. This small protein is expressed by *V. cholerae* and other naturally transformable bacteria. In these organisms ComEA plays an important role in horizontal gene transfer as it is required for the uptake of extracellular DNA from the extracellular media, thereby contributing to genome plasticity and bacterial evolution.[42] The protein has two lysine residues, which are positively charged and shown to be crucial for DNA-binding. The total charge of recombinant tagged ComEA with ProteinCalculator v3.4 gave a total charge of −3 at pH 8.0.[42] Until now, DNA–protein interactions were only studied using classical silicon-nitride nanopores which examined proteins

such as RecA (38 kDa), P19 (16 kDa) and the histone monomer (14 kDa).[40,43–45] This is therefore the first detection of such a small DNA-binding protein of only 12 kDa, using glass nanopores.

Materials and methods

The quartz capillaries were purchased with an inner and outer diameter of 0.3 and 0.5 mm (Hilgenberg, Germany). The capillaries were pulled with the laser pipette puller P-2000 (Sutter, USA). The pulling parameters were heat 620, filament 0, velocity 30, deletion 140, and pull 200 resulting in a single pull after an activated laser for approximately 1.1 seconds. This resulted in nanocapillaries with a taper length of approximately 4 mm. A detailed description of the capillary pulling can be found in previous publications.[24,26,38]

The resulting nanocapillaries from the pull were imaged under a field emission scanning electron microscope (FESEM). The Merlin SEM (Zeiss, Germany) did not necessitate the presence of a conducting layer on the glass nanocapillaries when imaging took place with the in-lens detector. The SEM imaging and shrinking were performed at a working distance of approximately 3 mm, magnifications between 100 kX and 250 kX, beam currents of about 500 pA and acceleration voltages of 2 kV.[38]

The nanocapillaries were assembled into a PDMS cell, whose two reservoirs were connected only by the glass orifice. The bottom of the PDMS cell was sealed with a 0.15 mm thick cover glass (Menzel-Glässer, Germany). The reservoirs were filled with a KCl solution of 1 mol L^{-1} (M), 1 mM Tris, and 0.1 mM ethylenediaminetetraacetic acid (EDTA) buffered at pH 8. The solution was cleared from any contaminating particles using an Anotop 25 filter (Watman, USA). To ease filling with the KCl buffer, a quartz glass was rendered hydrophilic by oxygen plasma cleaning for five minutes. After the addition of the buffer solution, the PDMS cell was degassed inside a desiccator using a vacuum pump, which removed obstructing air bubbles inside the conical part of the glass nanopores.[26] The conductance of the cells was measured by taking a standard current–voltage (IV) curve. Voltages up to ±800 mV were applied with incremental steps of 50 or 100 mV. The linear fit of the resulting ionic current revealed the conductance (G).

An Axopatch 200B current amplifier was used (Axon Instruments, USA) to apply potentials up to ±1 V and measure ionic currents up to 200 nA. The Bessel filter frequency was held constant at 10 kHz. A PXI-4461 DAQ card (National Instruments, USA) was used to sample the filtered current at a frequency of 100 kHz which was recorded by a custom LabVIEW program. The silver electrodes were chlorinated (Ag/AgCl) by applying a DC potential of 2 V in a 1 M KCl solution to reduce the surface resistance of silver. The grounded electrode was positioned on the *cis* side in front of the glass nanopore while the working electrode was placed on the opposite, *trans* side (Fig. 1a). The IV curves and events were recorded using the custom LabVIEW program which also allowed the recording of the full ionic current trace or trigger recording once the ionic current depreciated under a user-defined level. The recorded events were analyzed using the free OpenNanopore software.[46]

The DNA translocation experiments were carried out in a KCl solution of 1 M, 1 mM Tris, and 0.1 mM EDTA buffer at pH 8. 48.5 kbp long λ-DNA was purchased from New England Biolabs (USA) in a concentration of 0.5 μg μL^{-1} and diluted to 2.5 ng μL^{-1} in the 1 M KCl buffer solution. 50 μL were added to the *cis* chamber and a potential of +0.5 V was applied to the electrode in the opposite *trans* chamber.

Samples for protein translocations were prepared specifically for each protein. RNA polymerase was purchased from New England Biolabs (USA). RNAp was diluted in 1 M KCl, Tris-EDTA with a pH of 8.0 to a concentration of 0.6 μM. BSA was purchased by Acros Organics (USA). The protein was diluted in 1 M KCl, buffered in Tris EDTA (pH 8.0 or pH 2.5) to a concentration of 0.6 μM. Green fluorescent protein (GFP) was purchased from Evrogen (Russia) as rTurboGFP in a concentration of 1 μg μL^{-1} (0.037 M) and stored at 4 °C. For the translocation experiment, the GFP (27 kDa) was diluted to a concentration of 37 μM in a 1 M KCl, 1 mM Tris, 0.1 mM EDTA, and pH 8.0 solution. The fusion protein was PSCFP2-PAmCherry1. Its gene was cloned into an expression cassette downstream of a T7 promoter and a 6XHis region into a pRSET A vector. The construct was purchased from DNA 2.0 (DNA 2.0 plasmids ID 65603). More details of the purification of the PSCFP2-PAmCherry1 can be found in the ESI.† The purified FP was diluted to 9 μM in 1 M KCl, 1 mM Tris, 0.1 mM EDTA, and pH 8.0. IgG anti TAG antibody was purchased from BioConcept (Switzerland) and diluted to 0.6 μM in 1 M KCl, 1 mM Tris, 0.1 mM EDTA, and pH 8.0. ComEA was provided by the group of Blokesch and was diluted to a 0.6 μM by a 1 M KCl,1 mM Tris, 0.1 mM EDTA, and pH 8.0 solution.[42] The protein was mixed with 800 bp long DNA before translocating it with a potential of 0.5 V.

Results and discussion

The charge of a protein depends on its environment. In particular, the pH of the buffer in which the protein is maintained plays a crucial role. The pI of the protein is the pH of the buffer where the net charge on the amphoteric molecule is neutral. When the protein is placed in a buffer solution above its pI value, the net charge is negative and below the pI value the protein exhibits a net positive charge. When the pH of a solution is charged, it can reverse the translocation direction of a protein as shown by Firnkes *et al.* and Han *et al.* with avidin and BSA in silicon nanopores, respectively.[6,7] Fig. 2 demonstrates the use of glass nanopores to detect the reversal of surface charges on BSA at different pH levels.[47] At this pH, the BSA has a negative charge and therefore shows no translocation events at −0.8 V (Fig. 2a), while showing spikes at a positive potential (Fig. 2b). At pH 2.5 BSA has a net positive charge reversing the previous observation, which is visible in

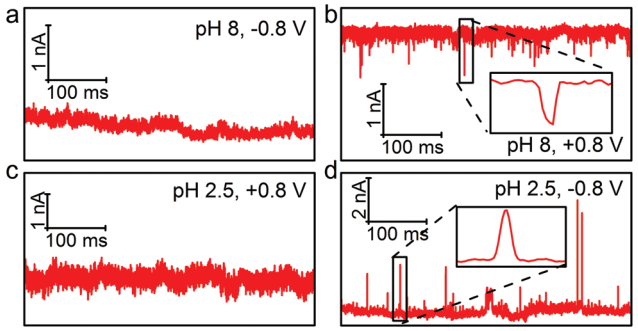

Fig. 2 (a) Current trace measured across the pore at pH 8 and a negative voltage of −0.8 V. Note the absence of events as BSA is negatively charged at this pH and does not enter the pore when a negative field is applied. (b) Trace of the current when a positive voltage of 0.8 V is applied at pH 8. Numerous events show the passage of BSA molecules through the pore. Inset shows a magnified typical event. (c) Current trace at an applied potential of +0.8 V and pH 2.5. At a pH below the pI of 4.7, the BSA protein is positively charged and hence the protein does not translocate. (d) Current trace with pulses at −0.8 V and pH 2.5. Events are present in the form of peaks rather than dips at negative voltages. Inset shows typical event of positively charged BSA passing through the pore.

the eventless baseline at +0.8 V (Fig. 2c) and translocation events at a potential of −0.8 V (Fig. 2d).

Based on this finding, the same pH of 8 was used to detect negatively charged proteins with different molecular weights by translocating them through the glass nanopore using a positive potential. GFP (27 kDa), fusion protein (54 kDa), and lambda DNA was successfully translocated through the same glass nanopore, revealing differences in the blocked conductance (Fig. 3a, b and c). Electron irradiation from an SEM was used to shrink a 130 nm glass nanopore to 14 nm (see inset in Fig. 3a, b and c). The corresponding IV curve displayed a conductance of 36 nS which agrees with previous work.[38] GFP was added to the *cis* side and a potential of 0.5 V was generated to induce the passage of the protein through the glass nanopore. Again, the average amplitude was determined using a Gauss fit to the histogram, returning a value of −0.22% (Fig. 3a). The *cis* chamber was flushed with a 1 M KCl solution to remove the protein. Its removal was tested by an event-less current baseline, when the potential of 0.5 V was applied (see ESI Fig. 1b†). FP was then added to the *cis* side and translocated to the *trans* side by applying a potential of 0.5 V, which triggered events caused by the transient blocking of the current by the protein inside the glass nanopore (Fig. 3b). The average position of −0.48% was determined by fitting the small peak in the histogram to a Gauss function (see dashed line in the histogram of Fig. 3b). This increase in the blocked conductance relative to the smaller GFP protein was anticipated since FP is twice as big as GFP. As before, the *cis* reservoir was washed with a 1 M KCl solution resulting in an event-less current baseline (see ESI Fig. 1c and d†). As a positive control, λ-DNA was translocated (2.5 ng μL^{-1} in 1 M KCl), which is known to show quantized events.[24] They occurred in a step-like pattern which is visible in the histogram of Fig. 3c. The first peak has a con-

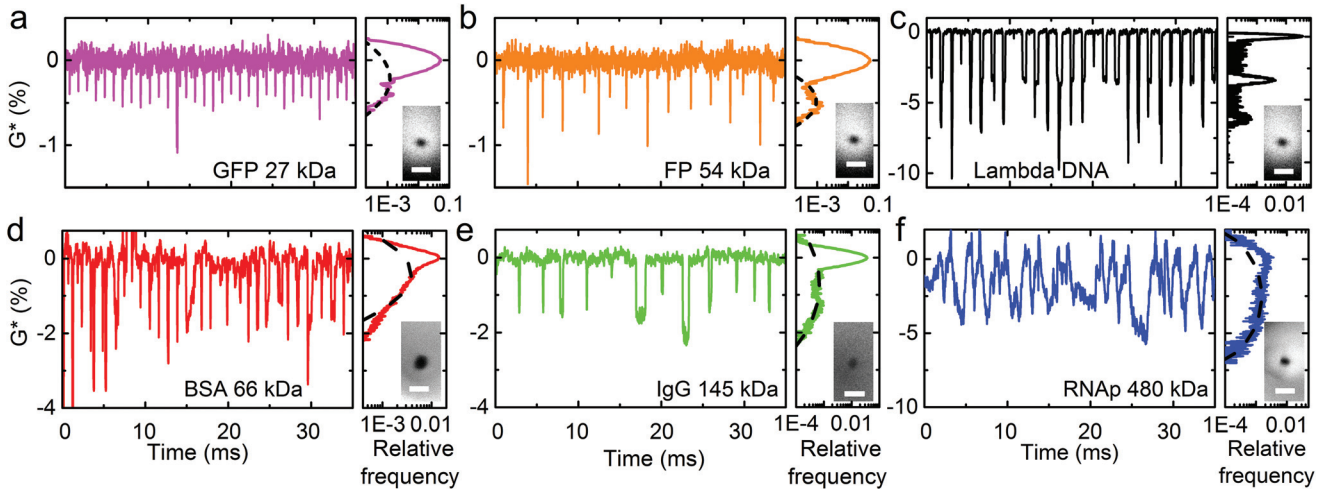

Fig. 3 All translocations were done at 0.5 V in a 1 M KCl solution. For better comparison with the other translocated proteins the ionic current is displayed as concatenated traces divided by the base line current (*G**). All scale bars in the SEM image are 50 nm long. (a) Addition of the GFP to the *cis* side caused translocation of the protein detectable by the spike-like depreciations of the ionic current. The right graph shows the histogram of the *G** curve revealing a small peak at 0.22% fitted with a Gaussian function (dashed line). The inset shows the respective 14 nm nanopore. (b) *G** trace while translocating FP through the glass nanopore. Again peaks are observed, which is apparent in the right histogram with a peak at around 0.48%. The inset shows the same glass nanopore as in (a). As a positive control experiment, λ-DNA was translocated across the identical glass nanopore, revealing clear translocation events observed in the step-like decrease in the *G** trace apparent, as peaks in the adjacent histogram. Again the SEM inset is the same as in (a) and (b). (d) *G** trace with BSA translocation peaks. Fitting of a Gauss function to the side peak in the histogram positioned the BSA peak at 0.44%. The inset shows the shrunken glass nanopore with a diameter of 21 nm. (e) *G** trace displaying IgG translocation, the corresponding histogram shows a peak at 0.71% revealed by the Gauss fit (dashed line). Inset shows SEM image of the glass nanopore after shrinking to a diameter of 16 nm. (f) *G** curve after the addition of RNAp to the *cis* side. The broad peak caused by the RNAp translocation in the adjacent histogram was located at 2.52% using a Gauss fit. Inset shows the SEM image of the glass nanopore after shrinking, revealing a diameter of 13 nm.

ductance value around −3% or 1.3 nS. This conductance value for a 14 nm nanopore falls in the expected range with a previously published value of 1.7 nS for a similar small glass nanopore.[37] This confirms the small size of the glass nanopore and supports the ability to detect minuscule molecules such as GFP with only 27 kDa.

Afterwards, BSA (66 kDa), IgG (145 kDa), and RNAp (480 kDa) were translocated across similar sized glass nanopores. The insets in Fig. 3d, e and f show the electron induced shrinking of the glass nanopores to diameters of 21, 16, and 13 nm, respectively. This diameter range is slightly bigger than the proteins having diameters of 5.4, 6.9, and 10.5 nm when approximated as a sphere (see ESI Fig. 2† for illustration). The IV-curves indicated a conductance of 97, 127, and 11 nS, respectively. As for the previous proteins, BSA, IgG, and RNAp were translocated at a potential of 0.5 V. The fit with the Gauss function revealed values of 0.44% for BSA, 0.71% for IgG and 2.52% for RNAp (see dashed line for fit in the histogram Fig. 3d, e and f).

Reassured by the detection of this wide spectrum of proteins, the ability of the protein ComEA to bind DNA was tested. Recombinant ComEA has a molecular weight of only 12 kDa. In order to detect its DNA-binding capabilities, a nanopore was shrunk from 260 to 21 nm (Fig. 4a). The linear fit to the IV-curve revealed a conductance of 51 nS (Fig. 4b). First, only 800 bp DNA was translocated using a potential of 0.5 V. This caused spike-like events showing decreases in the current, which was anticipated due to the small length of the dsDNA molecule (Fig. 4c). This is the shortest DNA molecule detected until now using glass nanopores. A Gauss function was used to fit the peak caused by the translocation molecule, locating it at −0.42%. Then, the DNA was incubated with ComEA and flushed into the *cis* reservoir. A potential of 0.5 V was applied, which caused the translocation of the ComEA-DNA complex (Fig. 4d). The fractional conductance blockade was determined using a Gauss fit at −0.7% (see dashed line in histogram Fig. 4d). This showed a difference of 0.28% in the G^* value between the bare DNA and the DNA-ComEA complex.

The proteins were analyzed quantitatively by calculating the duration and peak amplitudes for the previously discussed proteins. The latter was calculated by dividing the deepest conductance drop by the total conductance of the nanocapillary. This value is referred to as the normalized conductance drop. As expected, their distribution shifts to larger normalized conductance drops with higher molecular weights (Fig. 5a–e). GFP representing the smallest protein shows a narrow distribution from 0 to 0.5 ms whereas larger proteins such as BSA, IgG, and RNAp show broader distributions from 0 to 1 ms, 0 to 1.5 ms, and 0 to 3 ms, respectively. To display the center of highest density, an R script was used to assign each point a value depending on its number of neighbors. Red depicts a region of high density while blue shows a region with low density. The center for each distribution was determined by calculating its mean as well as variance and was plotted for all five proteins in Fig. 5f. A clear trend is observed showing higher normalized conductance drops with increasing molecular weights. The same trend is observed for the duration except for the GFP and the FP, where the latter show a smaller duration. This discrepancy may be due to the fact, that GFP and FP are small proteins compared to BSA, IgG, and RNAp. The small size of a couple of nanometers in combination with the glass nanopores having diameters of about 20 nm could impede the correct determination of the duration of the events. Better results for similar sized proteins could be obtained by classical nanopores embedded in thin membranes as shown previously by Larkin *et al.*[48] Another reason for the

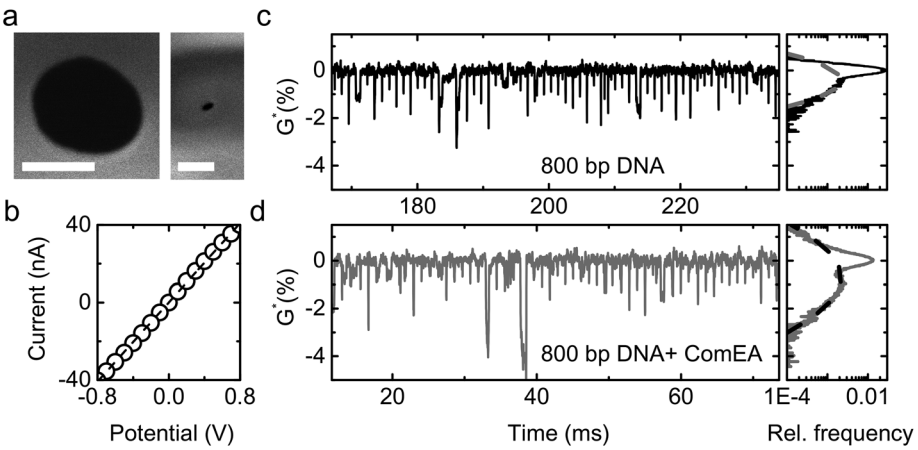

Fig. 4 (a) SEM image of the glass nanocapillary before (diameter 260 nm) and after shrinking (diameter 21 nm). Both white scale bars are 100 nm. (b) IV curve of the shrunken nanopore shown in (a) whose linear fit revealed a conductance of 51 nS. (c) After the addition of 800 bp long DNA, translocation events with decreasing G^* values were observed at a potential of 0.5 V in 1 M KCl. The right histogram shows the frequency count of the recorded trace with a peak besides the baseline current. This was fitted with a Gauss curve (grey dashed line) with a center at −0.42%. (d) After flushing with 1 M KCl and adding 800 bp long DNA incubated with ComEA protein to the *cis* side, translocation events with decreasing G^* values were observed at a potential of 0.5 V. The smaller side peak in the right histogram was fitted with a Gauss curve (grey dashed line) having a center at −0.7%.

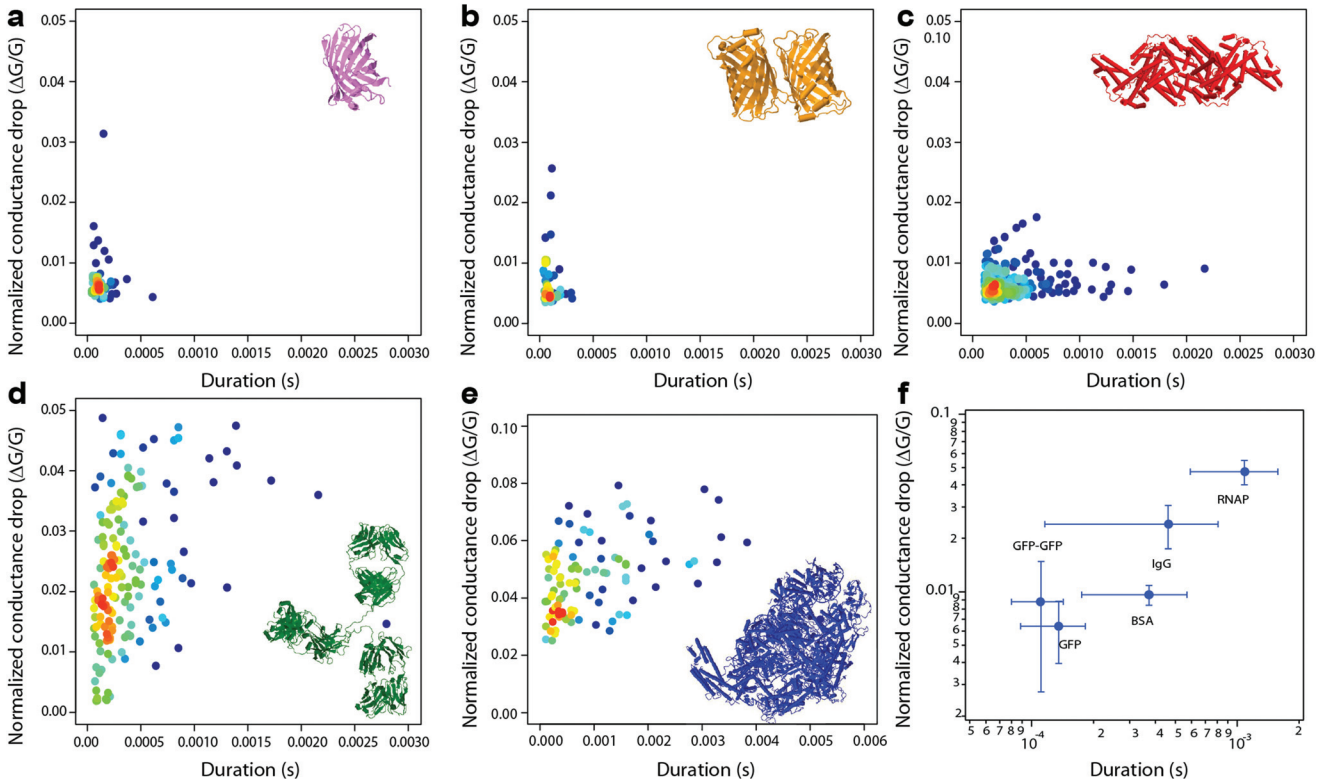

Fig. 5 Scatter plots resulting from the translocation of the five proteins GFP (a), FP (b), BSA (c), IgG (d), and RNAp (e) showing 60, 49, 236, 168, and 92 events, respectively. Although the event number for the first two proteins is relatively low. Rigorous control experiments included washing and detecting λ-DNA to support the validity of the data (see Fig. S3†). The *x*-axis represents the duration in seconds while the *y*-axis shows the normalized conductance drop. The latter is calculated by dividing the peak current amplitude of each event with its potential and the overall conductance of the cell. An algorithm written in R to calculate a density heat plot allowed a color for the assignment of every event, depending on its distance from the center. (f) The centers of gravity for GFP (27 kDa), FP (54 kDa), BSA (66 kDa), IgG (145 kDa), and RNAp (480 kDa) obtained from the previous scatter plots show a continuous increase in the normalized conductance drop with increasing molecular weights.

discrepancy in the duration may be the surface of the nanopores, which is extremely important for the interaction between proteins and nanopores. These interactions can determine the sensitivity and the duration of protein translocations. The discrepancy in duration may also be the low number of events for GFP and FP of 60 and 49, respectively. Nevertheless, the overall trend of a longer duration and higher normalized conductance drops for higher molecular weights are clearly visible for the proteins BSA, IgG, and RNAp. An alternative analysis, supporting this trend, was done by fitting a Gauss function to the normalized conductance traces showing translocation events of the proteins (see ESI Fig. 3†). The fit showed an increasing conductance drop for larger proteins in line with the results from the scatter plot, where bigger proteins cause bigger conductance blockades.

Conclusions

This research demonstrates the capability of glass nanopores to measure the size of proteins by detecting the fractional conductance drop. The ability to shrink the glass nanopores to similar dimensions as the protein size by electron irradiation, was essential. The detection of proteins using shrunken glass nanopores for proteins ranging from 12 to 480 kDa was demonstrated. This range is slightly larger than the protein size range used in a similar setup using glass nanocapillaries published by Li *et al.*, while our measurements were done at a constant Bessel filter frequency of 10 kHz.[36] The ability to shrink glass nanopores has important advantages like tailoring the glass nanopore diameter to the size of the target molecule (ESI Fig. 2†). Besides demonstrating the ability to detect the size of the protein using the fractional conductance blockade, it was also possible to flip the translocation direction of the protein by changing the pH. The research also showed the possibility of investigating DNA–protein interactions between DNA and the ComEA protein. In the future nanopores will be shrunk using techniques such as helium ion microscopes or atomic layer deposition (ALD) to dimensions below 5 nm. Moreover, the high bandwidth and low noise of the novel current amplifier, Chimera, will be used to detect even smaller single molecules such as single stranded DNA.[49] All these measurements will improve the SNR allowing detection of short single stranded DNA molecules and proteins smaller than 10 kDa.[44,50]

Acknowledgements

This work and LJS were financially supported by the European Research Council (grant no. 259398, ProABEL: Nanopore integrated nanoelectrodes for biomolecular manipulation and design to AR) and the Swiss National Science Foundation (grant no 31003A_143356 to MB). We thank the valuable input from Helen Chong Horrigan.

Notes and references

1 J. Li, D. Stein, C. McMullan, D. Branton, M. J. Aziz and J. A. Golovchenko, *Nature*, 2001, **412**, 166–169.
2 J. Li, M. Gershow, D. Stein, E. Brandin and J. A. Golovchenko, *Nat. Mater.*, 2003, **2**, 611–615.
3 A. Han, G. Schürmann, G. Mondin, R. A. Bitterli, N. G. Hegelbach, N. F. de Rooij and U. Staufer, *Appl. Phys. Lett.*, 2006, **88**, 093901–093903.
4 R. I. Stefureac, D. Trivedi, A. Marziali and J. S. Lee, *J. Phys.: Condens. Matter*, 2010, **22**, 454133.
5 D. S. Talaga and J. Li, *J. Am. Chem. Soc.*, 2009, **131**, 9287–9297.
6 M. Firnkes, D. Pedone, J. Knezevic, M. Döblinger and U. Rant, *Nano Lett.*, 2010, **10**, 2162–2167.
7 A. Han, M. Creus, G. Schürmann, V. Linder, T. R. Ward, N. F. de Rooij and U. Staufer, *Anal. Chem.*, 2008, **80**, 4651–4658.
8 D. Fologea, B. Ledden, D. S. McNabb and J. Li, *Appl. Phys. Lett.*, 2007, **91**, 539011–539013.
9 K. J. Freedman, S. R. Haq, J. B. Edel, P. Jemth and M. J. Kim, *Sci. Rep.*, 2013, **3**, 1–8.
10 C. Plesa, S. W. Kowalczyk, R. Zinsmeester, A. Y. Grosberg, Y. Rabin and C. Dekker, *Nano Lett.*, 2013, **13**, 658–663.
11 E. M. Nelson, V. Kurz, J. Shim, W. Timp and G. Timp, *Analyst*, 2012, **137**, 3020–3027.
12 D. Japrung, J. Dogan, K. J. Freedman, A. Nadzeyka, S. Bauerdick, T. Albrecht, M. J. Kim, P. Jemth and J. B. Edel, *Anal. Chem.*, 2013, **85**, 2449–2456.
13 L. Payet, M. Martinho, M. Pastoriza-Gallego, J.-M. Betton, L. Auvray, J. Pelta and J. Mathé, *Anal. Chem.*, 2012, **84**, 4071–4076.
14 K. J. Freedman, M. Jürgens, A. Prabhu, C. W. Ahn, P. Jemth, J. B. Edel and M. J. Kim, *Anal. Chem.*, 2011, **83**, 5137–5144.
15 R. Wei, V. Gatterdam, R. Wieneke, R. Tampé and U. Rant, *Nat. Nanotechnol.*, 2012, **7**, 257–263.
16 E. C. Yusko, J. M. Johnson, S. Majd, P. Prangkio, R. C. Rollings, J. Li, J. Yang and M. Mayer, *Nat. Nanotechnol.*, 2011, **6**, 253–260.
17 E. C. Yusko, P. Prangkio, D. Sept, R. C. Rollings, J. Li and M. Mayer, *ACS Nano*, 2012, **6**, 5909–5919.
18 S. Hernández-Ainsa, C. Muus, N. A. W. Bell, L. J. Steinbock, V. V. Thacker and U. F. Keyser, *Analyst*, 2013, **138**, 104–106.
19 M. M. Mohammad, R. Iyer, K. R. Howard, M. P. McPike, P. N. Borer and L. Movileanu, *J. Am. Chem. Soc.*, 2012, **134**, 9521–9531.
20 D. Rotem, L. Jayasinghe, M. Salichou and H. Bayley, *J. Am. Chem. Soc.*, 2012, **134**, 2781–2787.
21 M. Soskine, A. Biesemans, B. Moeyaert, S. Cheley, H. Bayley and G. Maglia, *Nano Lett.*, 2012, **12**, 4895–4900.
22 A. Oukhaled, B. Cressiot, L. Bacri, M. Pastoriza-Gallego, J.-M. Betton, E. Bourhis, R. Jede, J. Gierak, L. Auvray and J. Pelta, *ACS Nano*, 2011, **5**, 3628–3638.
23 A. H. Laszlo, I. M. Derrington, B. C. Ross, H. Brinkerhoff, A. Adey, I. C. Nova, J. M. Craig, K. W. Langford, J. M. Samson, R. Daza, K. Doering, J. Shendure and J. H. Gundlach, *Nat. Biotechnol.*, 2014, **32**, 829–833.
24 L. J. Steinbock, O. Otto, C. Chimerel, J. Gornall and U. F. Keyser, *Nano Lett.*, 2010, **10**, 2493–2497.
25 L. T. Sexton, L. P. Horne and C. R. Martin, *Mol. BioSyst.*, 2007, **3**, 667–685.
26 L. J. Steinbock and U. F. Keyser, in *Methods in Molecular Biology*, ed. M. E. Gracheva, Springer Science, Totowa, NJ, 2012, vol. 870, pp. 135–145.
27 P. Actis, A. McDonald, D. Beeler, B. Vilozny, G. Millhauser and N. Pourmand, *RSC Adv.*, 2012, **2**, 11638–11640.
28 B. Vilozny, P. Actis, R. A. Seger, Q. Vallmajo-Martin and N. Pourmand, *Anal. Chem.*, 2011, **83**, 6121–6126.
29 N. Laohakunakorn, B. Gollnick, F. Moreno-Herrero, D. G. A. L. Aarts, R. P. A. Dullens, S. Ghosal and U. F. Keyser, *Nano Lett.*, 2013, **13**, 5141–5146.
30 O. Otto, S. Sturm, N. Laohakunakorn, U. F. Keyser and K. Kroy, *Nat. Commun.*, 2013, **4**, 1780–1787.
31 N. Laohakunakorn, S. Ghosal, O. Otto, K. Misiunas and U. F. Keyser, *Nano Lett.*, 2013, **13**, 2798–2802.
32 T. R. Gibb, A. P. Ivanov, J. B. Edel and T. Albrecht, *Anal. Chem.*, 2014, **86**, 1864–1871.
33 X. Gong, A. V. Patil, A. P. Ivanov, Q. Kong, T. Gibb, F. Dogan, A. J. DeMello and J. B. Edel, *Anal. Chem.*, 2014, **86**, 835–841.
34 S. Polonsky, V. S. K. Balagurusamy and J. A. Ott, *Rev. Sci. Instrum.*, 2014, **85**, 084301.
35 J. S. Creamer, N. J. Oborny and S. M. Lunte, *Anal. Methods*, 2014, **6**, 5427.
36 W. Li, N. A. W. Bell, S. Hernández-Ainsa, V. V. Thacker, A. M. Thackray, R. Bujdoso and U. F. Keyser, *ACS Nano*, 2013, **7**, 4129–4134.
37 L. J. Steinbock, R. D. Bulushev, S. Krishnan, C. Raillon and A. Radenovic, *ACS Nano*, 2013, **7**, 11255–11262.
38 L. J. Steinbock, J. F. Steinbock and A. Radenovic, *Nano Lett.*, 2013, **13**, 1717–1723.
39 D. Pedone, M. Firnkes and U. Rant, *Anal. Chem.*, 2009, **81**, 9689–9694.
40 C. Raillon, P. Cousin, F. Traversi, E. Garcia-Cordero, N. Hernandez and A. Radenovic, *Nano Lett.*, 2012, **12**, 1157–1164.
41 O. A. O. Saleh and L. L. Sohn, *Rev. Sci. Instrum.*, 2001, **72**, 4449.

42 P. Seitz, H. Pezeshgi Modarres, S. Borgeaud, R. D. Bulushev, L. J. Steinbock, A. Radenovic, M. Dal Peraro and M. Blokesch, *PLoS Genet.*, 2014, **10**, e1004066.
43 S. W. Kowalczyk, A. R. Hall and C. Dekker, *Nano Lett.*, 2010, **10**, 324–328.
44 M. Wanunu, T. Dadosh, V. Ray, J. Jin, L. McReynolds and M. Drndić, *Nat. Nanotechnol.*, 2010, **5**, 807–814.
45 G. V. Soni and C. Dekker, *Nano Lett.*, 2012, **12**, 3180–3186.
46 C. Raillon, P. Granjon, M. Graf, L. J. Steinbock and A. Radenovic, *Nanoscale*, 2012, **4**, 4916–4924.
47 T. Estey, J. Kang, S. P. Schwendeman and J. F. Carpenter, *J. Pharm. Sci.*, 2006, **95**, 1626–1639.
48 J. Larkin, R. Y. Henley, M. Muthukumar, J. K. Rosenstein and M. Wanunu, *Biophys. J.*, 2014, **106**, 696–704.
49 J. K. Rosenstein, M. Wanunu, C. A. Merchant, M. Drndic and K. L. Shepard, *Nat. Methods*, 2012, **9**, 487–492.
50 G. M. Skinner, M. van den Hout, O. Broekmans, C. Dekker and N. H. Dekker, *Nano Lett.*, 2009, **9**, 2953–2960.